PAPER

Check for updates

Aqueous phase hydrogenolysis of glycerol with *in situ* generated hydrogen over Ni/Al$_3$Fe$_1$ catalyst: effect of the calcination temperature

Raquel Raso, [ID] Alejandro Lete, [ID] Lucía García, [ID] * Joaquín Ruiz, [ID] Miriam Oliva [ID] and Jesús Arauzo

The present work studied the influence of the calcination temperature on the aqueous phase hydrogenolysis of glycerol with *in situ* generated hydrogen over a Ni/Al$_3$Fe$_1$ catalyst. The Ni/Al$_3$Fe$_1$ catalyst was synthesized by the co-precipitation method at 28 mol% of Ni (Ni/(Ni + Al + Fe)) and a molar ratio of Al/Fe of 3/1. The prepared catalyst was calcined at different temperatures (500–750 °C). The obtained samples were tested for the aqueous phase hydrogenolysis (APH) of glycerol and characterized by several analytical techniques (ICP-OES, H$_2$-TPR, XRD, N$_2$-physisorption, NH$_3$-TPD, STEM, FESEM, and TGA). The catalyst calcined at 625 °C was selected as the best sample due to its high acidity, metal dispersion, and catalytic activity; 1,2-propanediol was the highest carbon selectivity product. In addition, it experienced lower metal leaching than the catalyst calcined at 500 °C.

Introduction

In recent decades, the consumption of fossil fuels has risen rapidly, resulting in an environmental crisis. The transport sector accounts for around 60% of global oil consumption and generates one-fifth of global CO$_2$ emissions.[1] The global atmospheric CO$_2$ concentration has increased in the last two decades from 369.38 ppm (2000) to 417.53 ppm (2022).[2] Therefore, developing sustainable and clean sources of combustibles is essential. In this context, biodiesel has become one of the most common worldwide biofuels.[1,2] Global biodiesel production soared from 36 billion liters in 2017 to 46.5 billion liters in 2020.[3] Biodiesel is mainly produced by the transesterification of triglycerides (animal fats, vegetable oils, and waste oils) using ethanol or methanol in the presence of a catalyst. However, for every 10 tons of biodiesel produced, around 1 ton of glycerol is generated as a by-product which can negatively affect its production costs.[4–6] Many works have been published on converting glycerol into value-added products, such as H$_2$ or 1,2-propanediol (1,2-PDO), to valorize the glycerol and improve the economics of biodiesel production.[7–9]

Among the various methods for glycerol conversion into valuable products, hydrogenolysis deserves special attention. Hydrogenolysis is a kind of reduction with hydrogen participation that allows obtaining products of industrial interest, such as 1,3-propanediol, 1,2-PDO, 1-propanol, 2-propanol, and ethylene glycol. In the work of Nakagawa and Tomishige,[10]

heterogeneous catalysts (noble and non-noble metal) for glycerol hydrogenolysis were reviewed, and mainly 1,2-PDO was produced.

The conversion of glycerol to 1,2-PDO emerges as an attractive alternative because the 1,2-PDO market can absorb large quantities of glycerol.[11] In this case, the aqueous phase hydrogenolysis (APH) of glycerol to 1,2-PDO can be carried out without external hydrogen addition. In this process, hydrogen is generated *in situ* from glycerol reforming, making it safer and less expensive than conventional glycerol hydrogenolysis. Traditional hydrogenolysis of glycerol in the liquid phase requires H$_2$ feeding. APH without external hydrogen addition is a catalytic process carried out at moderate pressures of around 34 bar and relatively low temperatures of around 227 °C, obtaining gas and liquid products from a renewable feedstock.[12]

Nickel-based catalysts are attractive materials for use in the APH of glycerol because of their accessibility, high reactivity, low price, and high activity for producing H$_2$, which is an advantage for the hydrogenation reaction. They can break the C–C bond efficiently towards ethylene glycol production. The use of hydrogen generated *in situ* from glycerol reforming makes hydrogenolysis a more "green" process since hydrogen is usually derived from fossil fuels.[13–15]

Most of the works published in the literature related to glycerol hydrogenolysis without external hydrogen use batch reactors (discontinuous feeding).[16–20] Few studies have reported continuous operations that could be useful due to their more significant production potential on an industrial scale.[12]

Some works, such as those of Cai *et al.*[21] and Freitas *et al.*,[13] studied the APH of glycerol with and without the addition of external hydrogen in a fixed-bed reactor using bimetallic Ni/Cu

Thermochemical Processes Group (GPT), Aragon Institute of Engineering Research (I3A), Universidad de Zaragoza, Mariano Esquillor S/N, 50018 Zaragoza, Spain. E-mail: luciag@unizar.es

catalysts. Freitas et al.[13] found that the bimetallic Ni–Cu catalysts (CuNi/Al$_2$O$_3$ and CuNi/ZSM-5) showed the highest glycerol conversion with a 1,2-PDO yield of around 25% without external hydrogen addition. They also concluded that the presence of Ni is significant for glycerol reforming, obtaining in situ H$_2$ that is used to generate 1,2-PDO from acetol hydrogenation. Cai et al.[21] proposed the same reaction pathway for glycerol hydrogenolysis with and without external hydrogen addition on Ni/Cu/TiO$_2$ catalysts which included the dehydration of glycerol to produce acetol and the hydrogenation of acetol to achieve 1,2-PDO.

More recently, Mendonça et al.[22] studied the effect of MgO addition to Cu–Ni/Al$_2$O$_3$ catalysts on glycerol hydrogenolysis in a continuous reactor without external hydrogen addition. They observed the highest selectivity to 1,2-PDO of about 50% with the Cu–Ni/30 wt% MgO–Al$_2$O$_3$ catalyst after 6 h of reaction.

Our previous study[12] demonstrated that mixed-oxide catalysts (Ni/Al$_x$Fe$_y$) showed a better catalyst performance than Ni/Al and Ni/Fe catalysts, the Ni/Al$_3$Fe$_1$ catalyst being the best for the APH of glycerol in a continuous system without external hydrogen addition. A liquid carbon product selectivity to 1,2-PDO of around 71% was obtained. Besides this, the Ni/Al$_3$Fe$_1$ catalyst presented excellent activity for at least 9 h of reaction.[23]

The stability of the catalysts in aqueous processes under pressure, such as aqueous phase reforming (APR) and APH, is relevant for industrial use. The Ni/Al$_3$Fe$_1$ catalyst calcined at 500 °C and tested at 227 °C, and 34 absolute bar in the APH of glycerol showed boehmite formation and metal leaching.[12,23] The novelty of the present work is investigating the effects of the calcination temperature on the properties and catalytic activity of the Ni/Al$_3$Fe$_1$ catalyst for the APH of glycerol without external hydrogen addition. For this purpose, the coprecipitated Ni/Al$_3$Fe$_1$ catalyst was calcined at different temperatures (500–750 °C). The Ni/Al$_3$Fe$_1$ catalyst has the benefits of low cost, being a non-noble metal with high selectivity to 1,2-PDO, and stability for the APH of glycerol.[12,23]

Calcination is a relevant step in the preparation of the catalysts. The final calcination temperature influences their physicochemical properties, such as the surface area and crystallinity, affecting the catalytic performance. Moreover, the activation temperature of the catalysts determines their active metal phase, which is a key factor in catalytic activity.

As some examples, Bian et al.[24] studied the effect of the calcination temperature on the dry reforming of CH$_4$ over Ni-based catalysts. They found the highest activity at an intermediate calcination temperature. They concluded that the formation of NiAl$_2$O$_4$ spinel was beneficial to the activity and stability. Similar tendencies were obtained by Barzegari et al.[25] in the dry reforming of propane. They found that the calcined sample at 600 °C displayed the best catalytic performance with the highest Ni dispersion and surface area combined with sufficient basicity.

Ozdemir et al.[26] showed that for catalyst systems where there is no interaction between metal oxide components and the support, calcination at high temperatures is beneficial for obtaining catalysts with an excellent dispersion if spinel or solid solution formation occurs during the catalyst preparation. In addition, calcination at low temperatures is helpful to prevent

NiO sintering. Thus, lower Ni particles and better dispersion are obtained after reduction. But these phenomena are unclear for catalyst systems in which there is an interaction between their components.

To the best of our knowledge, there are few studies about the influence of the calcination temperature on the catalyst employed, such as ZnPd/ZnO–3Al, Os/bentonite, and Cu–Fe in glycerol hydrogenolysis to 1,2-PDO,[27–29] and the effect on the Ni/Al$_3$Fe$_1$ catalyst has not been previously studied.

The Ni/Al$_3$Fe$_1$ catalyst is a promising catalyst for the APH of glycerol. Studying its calcination temperature is relevant to optimizing the catalyst preparation conditions that could improve its catalytic performance. For these purposes, APH of glycerol without external hydrogen addition experiments were carried out in a continuous installation, and the catalysts were characterized before and after the reaction.

Experimental

Catalyst preparation and characterization

Ni/Al$_3$Fe$_1$ catalyst was prepared by the co-precipitation method at a 28 mol% of Ni (Ni/(Ni + Al + Fe)) and a molar ratio of Al/Fe of 3/1. The catalyst was calcined at different temperatures (500–750 °C, denoted as Ni/Al$_3$Fe$_1$-X, X being the calcination temperature in °C) for 3 h in order to study the influence of the calcination temperature on the APH of glycerol. Moreover, it was characterized by many techniques: inductively coupled plasma optical emission spectrometry (ICP-OES), hydrogen temperature-programmed reduction (H$_2$-TPR), X-ray diffraction (XRD), temperature-programmed desorption of ammonia (NH$_3$-TPD), thermogravimetric analysis (TGA), N$_2$-physisorption, scanning transmission electron microscopy (STEM), and field emission scanning electron microscopy (FESEM). The detailed procedures for the catalyst preparation and characterization are described in our previous work.[12]

Catalyst performance

Catalytic performance was examined in a continuous system (Process Integral Development Eng & Tech, Spain) which mainly consisted of a stainless-steel fixed bed reactor with an inner diameter of 9 mm, and a micrometric valve that regulated the pressure system. The fixed bed was composed of a mixture of catalyst (2 g) and sand (5 g), and their mesh sizes were 160–315 μm. It was placed on a tubular reactor and covered with quartz wool supports. Before the catalytic test, the catalysts were reduced, according to the H$_2$-TPR results.

A solution of 10 wt% glycerol (Sigma-Aldrich, purity: 99.5%) in deionized water was pumped into the reactor at 1 mL min^{-1}. The reaction occurred at 227 °C and 34 absolute bar for 3 h. Gas and liquid products were obtained during the APH of glycerol under these operating conditions. The products leaving the reactor were depressurized using the micrometric valve and arrived at the condensation system, where the liquid products were collected. The exit gas mixture: N$_2$, C$_2$H$_6$, CH$_4$, H$_2$, CO, CO$_2$, and C$_3$H$_8$, where N$_2$ was used as an internal standard, was analyzed online using an Agilent 490 Micro-GC equipped with

Thermal Conductivity Detectors (TCD). The liquid products consisted mainly of methanol (MeOH), acetol, ethanol (EtOH), acetic acid, ethylene glycol (EG), 1,2-propanediol (1,2-PDO), and non-reacted glycerol. They were examined offline using an Agilent 7820A GC equipped with a Flame Ionization Detector (FID) and an HP-FFAP Agilent 19091F-105 capillary column. 1-Butanol (PanReac, purity: 99.5%) was used as an internal standard. Besides, the liquid products were submitted to an inductively coupled plasma optical emission spectrometry (ICP-OES) analysis to examine the possibility of metal leaching. More details of the experimental system were described in our earlier studies.[12,23] The catalytic performance (glycerol conversion, carbon yield to gases and liquids) was calculated as follows, according to the expressions cited in our previous studies:[12,23]

$$\text{Glycerol conversion (\%)} = \frac{n_{\text{glycerol}}^{\text{in}} - n_{\text{glycerol}}^{\text{out}}}{n_{\text{glycerol}}^{\text{in}}} \times 100$$

where $n_{\text{glycerol}}^{\text{in}}$ are the total moles of glycerol fed and $n_{\text{glycerol}}^{\text{out}}$ are the total moles of unreacted glycerol in the exit liquid.

$$\text{Carbon yield to gases (\%)}$$
$$= \frac{n_{\text{CO}} + n_{\text{CO}_2} + n_{\text{CH}_4} + 2n_{\text{C}_2\text{H}_6} + 3n_{\text{C}_3\text{H}_8}}{3 \times n_{\text{glycerol}}^{\text{in}}} \times 100$$

$$\text{Carbon yield to liquids (\%)} = \frac{n_{\text{MeOH}} + 2n_{\text{EtOH}} + 2n_{\text{acetic acid}} + 3n_{\text{acetol}} + 3n_{\text{1,2-PDO}} + 2n_{\text{EG}}}{3 \times n_{\text{glycerol}}^{\text{in}}} \times 100$$

where n_i are the total moles of the i product (i = liquid or gas). The carbon selectivity to products (gases and liquids) was defined as the percentage ratio of carbon in a product 'i' to the total carbon in all the analyzed products (gases and liquids), excluding the unreacted glycerol.

Due to errors in analyzing and collecting the samples, there was no complete coincidence between the glycerol conversion and the addition of the carbon yield to products (gas and liquid). As reported by other authors,[12,17,30] an experiment with a value of carbon deficit below 15% was considered a reliable test. The carbon deficit was defined as follows:

Carbon deficit = glycerol conversion
          − (carbon yield to gases + carbon yield to liquids)

Results and discussion

Catalytic performance experiments

Glycerol conversion, carbon yield to gases, and carbon yield to liquids are shown in Fig. 1. More carbon yield to liquid than carbon yield to gas was obtained for all samples; therefore, the operating conditions favored liquid production.[12,30] There were slight differences between the Ni/Al₃Fe₁-500 and the Ni/Al₃Fe₁-
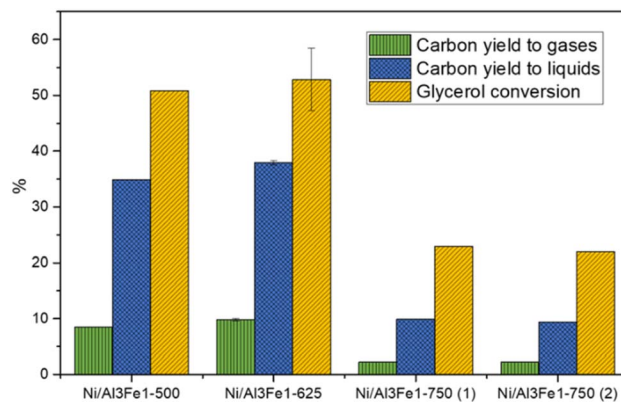

Fig. 1 Glycerol conversion, carbon yield to gases, and carbon yield to liquids.

625 catalysts, calcined at 500 °C and 625 °C, respectively. However, the Ni/Al₃Fe₁ catalyst calcined at 750 °C showed the worst catalytic activity. For example, the carbon yield to liquids was around 38% for the Ni/Al₃Fe₁-625 catalyst, while for the catalysts calcined at 750 °C (Ni/Al₃Fe₁-750 (1) and Ni/Al₃Fe₁-750 (2)), it was about 10%.

Prior to the catalytic test, the Ni/Al₃Fe₁-500 and Ni/Al₃Fe₁-625 catalysts were reduced at 500 °C, but the Ni/Al₃Fe₁-750 was activated at 650 °C (Ni/Al₃Fe₁-750 (1)), according to the H₂-TPR results. Due to the low catalytic performance of the catalyst calcined at 750 °C and reduced at 650 °C, this catalyst was also reduced at 725 °C (Ni/Al₃Fe₁-750 (2)) in order to improve its performance. However, there was no improvement obtained in their catalytic performance.

Fig. 2(A) displays the gas compositions (vol%, N₂, and H₂O free). The exit gas was composed mainly of CO₂ and H₂ and low amounts of CH₄, C₂H₆, and C₃H₈. The low content of CO is expected due to the water–gas shift (WGS) reaction being carried out at a low temperature.

The content of H₂ in the gas stream was boosted by increasing the calcination temperature, while the CO₂ was almost unchanged. In addition, the alkanes (CH₄, C₂H₆, and C₃H₈) were diminished, and CO was practically not found.

For the Ni/Al₃Fe₁ catalyst calcined at 750 °C, boosting the reduction temperature from 650 (Ni/Al₃Fe₁-750 (1)) to 725 °C (Ni/Al₃Fe₁-750 (2)) favored the decrease in the content of CO₂ and alkanes but increased that of H₂.

Fig. 2(B) shows the carbon selectivity to products for the catalysts tested, including gas and liquid products. All catalysts presented around 20% and 80% of converted carbon in gas and liquid products, respectively. The gas product with the highest carbon selectivity was CO₂. This was about 16% and almost
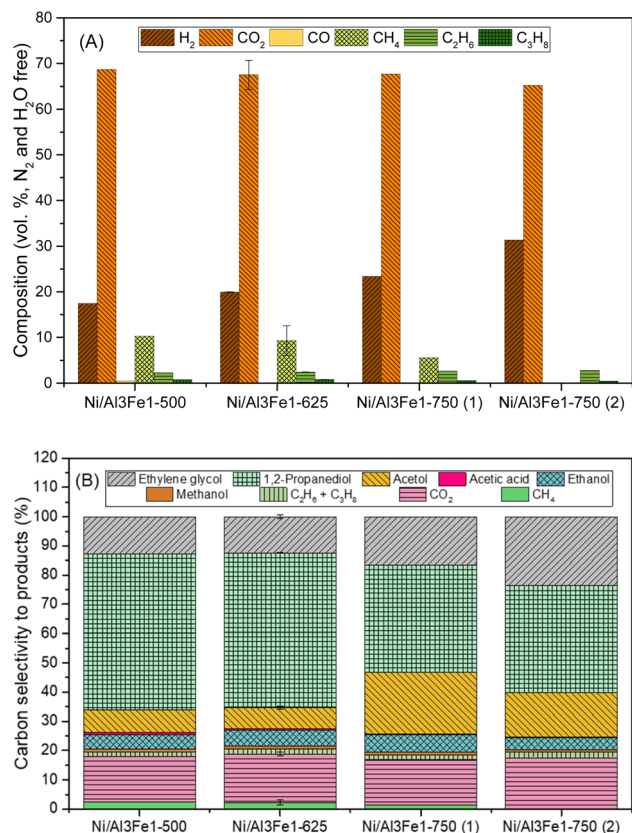
Fig. 2 Gas composition (vol%, N_2, and H_2O free) (A) and carbon selectivity to products (B).

unchanged with the calcination temperature. Meanwhile, the alkanes (CH_4, C_2H_6, and CH_3H_8) decreased, and CO was practically not found.

The major liquid products were 1,2-PDO, acetol, and ethylene glycol. 1,2-PDO was the product with the highest carbon selectivity among liquid and gas products, with values up to 53%. Garcia *et al.*[30] observed that when, for example, the APR of glycerol over Ni/Al catalyst occurred under the same operating conditions (34 bar, 10 wt% glycerol, and 227 °C), 1,2-PDO was the product with the highest carbon selectivity to liquid and gas products, with values around 37%. Roy *et al.*[17] also reported that 1,2-PDO was the product with the highest carbon selectivity, with values up to 53% obtained from the APH of glycerol over an admixture of 5% wt. Ru/Al_2O_3 and 5 wt% Pt/Al_2O_3 catalysts.

The carbon selectivity to 1,2-PDO, acetol and ethylene glycol did not change from Ni/Al_3Fe_1-500 to Ni/Al_3Fe_1-625. However, at a calcination temperature of 750 °C (Ni/Al_3Fe_1-750 (1)), the carbon selectivity to acetol and ethylene glycol increased, while the 1,2-PDO decreased. Meanwhile, increasing the reduction temperature for the Ni/Al_3Fe_1 catalyst calcined at 750 °C from 650 (Ni/Al_3Fe_1-750 (1)) to 725 °C (Ni/Al_3Fe_1-750 (2)) boosted ethylene glycol production, whereas the acetol was reduced, and the 1,2-PDO was unaffected.
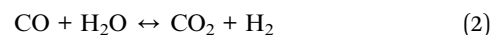
Considering the products obtained from the APH of glycerol without external H_2 addition and some references from the literature,[23,30–32] a proposed reaction mechanism is suggested in this work. The reaction network includes gas and liquid products.
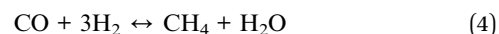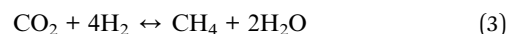
In the gas phase, H_2 and CO are mainly obtained by the reforming reactions of glycerol and liquid intermediates (eqn (1)) as well as by decarbonylation reactions that release CO. Then CO is converted into CO_2 and H_2 by the WGS reaction (eqn (2)). CH_4 is produced by the methanation reactions of CO and CO_2 (eqn (3)–(5)). In addition, Fischer–Tropsch reactions can explain the presence of C_2H_6 and C_3H_8.[30,31,33]

$$C_nH_mO_k + (n - k)H_2O \leftrightarrow nCO + (n + m/2 - k)H_2 \tag{1}$$

WGS reaction:

$$CO + H_2O \leftrightarrow CO_2 + H_2 \tag{2}$$

Methanation reactions:

$$CO_2 + 4H_2 \leftrightarrow CH_4 + 2H_2O \tag{3}$$

$$CO + 3H_2 \leftrightarrow CH_4 + H_2O \tag{4}$$

$$2CO + 2H_2 \leftrightarrow CH_4 + CO_2 \tag{5}$$

There are two main paths in the liquid phase:

In path I, glycerol is dehydrated into acetol, which is assumed to occur preferentially in acid sites. Subsequently, the hydrogenation of acetol produces 1,2-PDO using the H_2 generated *in situ*, which is expected to occur in metal sites (eqn (6)).[13,31,32,34]

In path II, glycerol is dehydrogenated to glyceraldehyde, whose further decarbonylation generates ethylene glycol (eqn (7)). Then, the dehydration and hydrogenation of ethylene glycol can produce ethanol. Besides, methanol is obtained by decarbonylation and dehydrogenation of ethylene glycol. Ethylene glycol can be dehydrated to form acetaldehyde. Acetaldehyde can be transformed into acetic acid. In addition, acetaldehyde can be hydrogenated to create also ethanol, which can be converted into this intermediate again by dehydrogenation.[17,23,30–33,35] It is worth noting that the reaction path to the formation of methanol can make glycerol produce more H_2.[31,32]

The experimental results indicated that using these catalysts and operating conditions, the main route is path I due to the high carbon selectivity to 1,2-PDO and acetol.

It is well known that the Ni active sites favor C–C bond cleavage and the WGS reaction. Furthermore, Ni exhibits activity for hydrogenation/dehydrogenation reactions.[30]

$$\tag{6}$$

$$\tag{7}$$
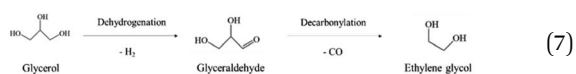
The catalysts calcined at low temperatures of 500 and 625 °C (Ni/Al$_3$Fe$_1$-500 and Ni/Al$_3$Fe$_1$-625, respectively) favored the dehydration reactions, which are assumed to occur in acid sites, and the hydrogenation reactions that take place in metal sites (path I). Thus, the carbon selectivity to 1,2-PDO and acetol together was around 60%, while the carbon selectivity to ethylene glycol was 12% for the Ni/Al$_3$Fe$_1$-625. In the APH of glycerol without external hydrogen addition, the catalyst must promote the dehydration of glycerol in acid sites to form acetol and simultaneously the reforming reaction for hydrogen production, which is required to generate 1,2-PDO by hydrogenation of acetol in metal sites.[13] Moreover, path II also takes place and explains ethylene glycol production. A clear trend could be observed by which an increase in the calcination temperature to 750 °C enhanced the dehydrogenation/decarbonylation reactions, promoting the formation of H$_2$, which requires metal sites (path II). In addition, the increase in the reduction temperature from 650 (Ni/Al$_3$Fe$_1$-750 (1)) to 725 °C (Ni/Al$_3$Fe$_1$-750 (2)) for the Ni/Al$_3$Fe$_1$ catalyst calcined at 750 °C encouraged the conversion of glycerol into dehydrogenation and decarbonylation products, increasing the selectivity to ethylene glycol and H$_2$. Thus, the carbon selectivity to 1,2-PDO and acetol together was 58% and 52% for the Ni/Al$_3$Fe$_1$-750 (1) and Ni/Al$_3$Fe$_1$-750 (2) catalysts, respectively, while the carbon selectivity to ethylene glycol was 17% and 24%, respectively.

Furthermore, the liquid products were submitted to ICP-OES analysis to examine the possibility of metal leaching. The Al, Ni, and Fe amounts 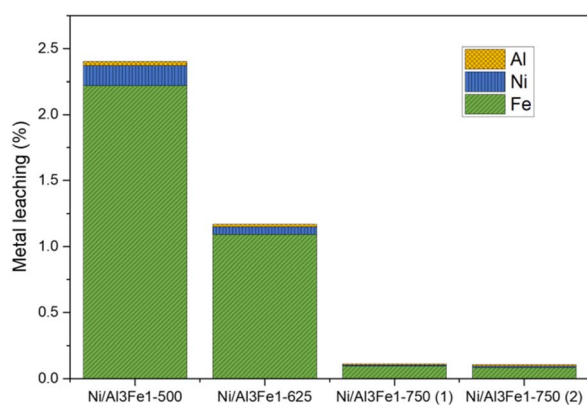detected in the liquid product are shown in Fig. 3. The metal leaching could be due to the dissolved CO$_2$ and/or soluble oxygenated compounds generated in the APH reaction of glycerol, such as acetic acid, which produces an acid medium.[35–37]

The metal leached to a lesser extent with an increase in the calcination temperature from 500 to 750 °C. Fe was the most leached and Al the least. The metal leaching was reduced by almost half from the Ni/Al$_3$Fe$_1$-500 to the Ni/Al$_3$Fe$_1$-625. Increasing the calcination temperature from 500 °C to 750 °C favored the excellent stability of the catalyst resulting in a smaller loss of its metals. The pH values of the collected liquid products were 4.0 and 4.4 for the catalysts calcined at 500 °C and 625 °C, respectively, and 5.6 and 5.5 for the catalysts calcined at 750 °C: Ni/Al$_3$Fe$_1$-750 (1) and Ni/Al$_3$Fe$_1$-750 (2), respectively. The results corroborate that the highest acidity of liquid products increased the metal leaching. Moreover, the acetic acid generated in the reaction was calculated, and the values were 4.1 mmol acetic acid/mol glycerol fed using the catalyst calcined at 500 °C; 3.6, 0.6, and 0.5 mmol acetic acid/mol glycerol fed using the catalysts Ni/Al$_3$Fe$_1$-625, Ni/Al$_3$Fe$_1$-750 (1) and Ni/Al$_3$Fe$_1$-750 (2), respectively. These data were in accordance with the pH values of the collected liquid products and demonstrated the effect of acetic acid in the acid medium.

Wu et al.[32] stated that acidic conditions boost the solubility of active metals in water, in agreement with the metal leaching results. The amount of metal leaching did not affect the catalytic activity of the samples under the operating conditions, as also reported by Raso et al.[23] However, a very high time-on-stream could influence the catalytic activity. It is better to develop a catalyst with low metal leaching.

It is well known that Ni catalysts supported on Al$_2$O$_3$ are often unstable and suffer changes in their structure during the APR of glycerol, causing deactivation by metal leaching, metal particles sintering, and so on.[14,36] Cai et al.[21] showed that the Ni/Cu catalyst suffered more deactivation by metal particles sintering and metal leaching when the glycerol hydrogenolysis was performed using water than 2-propanol as a solvent. However, the presence of Fe in catalysts helps to improve their stability and delays the deactivation of the Ni-based catalyst.[22,36]

In conclusion, the Ni/Al$_3$Fe$_1$-625 catalyst presented the best performance for the APH of glycerol due to its high catalytic activity towards dehydration/hydrogenation products and its lower degree of metal leaching than the Ni/Al$_3$Fe$_1$-500 catalyst under the same operating conditions.

Fig. 3 Metal leached after the APH of glycerol.

Table 1 Textural properties of the calcined and spent catalysts. Boehmite and FeNi$_3$ crystallite sizes of the used catalysts

Sample	Calcined samples			Spent samples				
	S_{BET}[a] (m^2 g^{-1})	V_p[b] (cm^3 g^{-1})	d_p[b] (nm)	S_{BET}[a] (m^2 g^{-1})	V_p[b] (cm^3 g^{-1})	d_p[b] (nm)	$D_{boehmite}$[c] (nm)	D_{FeNi_3}[c] (nm)
Ni/Al$_3$Fe$_1$-500	233	0.158	3.31	197	0.150	3.71	13	8
Ni/Al$_3$Fe$_1$-625	199	0.174	3.93	185	0.145	4.44	19	7
Ni/Al$_3$Fe$_1$-750 (1)	82[d]	0.145[d]	7.41[d]	56	0.126	13.10	15	11
Ni/Al$_3$Fe$_1$-750 (2)				42	0.136	18.70		20

[a] The Brunauer, Emmett, and Teller (BET) method. [b] Barrett–Joyner–Halenda (BJH) adsorption method. [c] Boehmite and FeNi$_3$ crystallite sizes calculated from the Scherrer equation. [d] Value corresponding to the Ni/Al$_3$Fe$_1$ catalysts calcined at 750 °C: reduced at 650 (1) and 725 °C (2).

Catalyst characterization

Chemical composition and textural properties. Almost no differences were found between the ICP-OES analysis and the nominal metal values in the Ni/Al$_3$Fe$_1$ catalyst. The

Fig. 4 N$_2$ adsorption–desorption isotherms of the calcined (A) and spent (B) samples. Pore size distribution of the calcined (C) and spent (D) samples.

experimentally measured Ni, Al, and Fe loading were 26.8 mol.% (nom.: 28.0 mol.%), 55.5 mol.% (nom.: 54.0 mol.%), and 17.7 mol.% (nom.: 18.0 mol.%), respectively.

The textural properties of the Ni/Al$_3$Fe$_1$ catalyst calcined at different temperatures are shown in Table 1. Fig. 4(A) and (B) show the N$_2$ adsorption–desorption of the calcined and used samples, respectively, and Fig. 4(C) and (D) display the pore size distribution of the calcined and used samples, respectively. According to the IUPAC classification, the fresh and spent catalysts exhibited a type IV isotherm with a hysteresis loop (type H$_2$) which occurred after $P/P_o = 0.4$. This is characteristic of mesoporous materials with interconnected pores of different sizes and shapes.[38] Boosting the calcination temperature decreased the surface area (S_{BET}) from 233 m^2 g^{-1} at 500 °C to 82 m^2 g^{-1} at 750 °C. It was 199 m^2 g^{-1} at 625 °C. The average pore diameter (d_p) increased, but the pore volume (V_p) had a maximum of 625 °C. In addition, it is observed that while the surface area and pore volume decreased after using the catalysts, the pore diameter increased. This trend could be because the samples suffered from pore plugging, which would have reduced their pore volume.[14]

A decrease in the S_{BET} was observed after using the samples. The catalysts calcined at 500 °C (Ni/Al$_3$Fe$_1$-500) and 625 °C (Ni/Al$_3$Fe$_1$-625) showed a slight decline in the S_{BET} and high catalytic activity. However, the Ni/Al$_3$Fe$_1$ catalysts calcined at 750 °C (Ni/Al$_3$Fe$_1$-750 (1) and Ni/Al$_3$Fe$_1$-750 (2)) demonstrated the highest decrease in the S_{BET} and the worst catalytic performance.

X-ray diffraction characterization. Fig. 5(A) shows the XRD patterns of the fresh samples. Peaks for spinel-structured FeAl$_2$O$_4$ (JCPDS, 00-034-0192) and NiAl$_2$O$_4$ (JCPDS, 00-010-0339) were observed in all samples. The interaction between NiO and Al$_2$O$_3$ forms the NiAl$_2$O$_4$ phase during the calcination, and its presence depends on the Ni/Al molar ratio and the calcination temperature.[39] The FeAl$_2$O$_4$ is obtained from the reaction of FeO with Al$_2$O$_3$.[40] Nonetheless, there were no peaks for FeO (JCPDS, 00-074-1886) and NiO (JCPDS, 00-047-1049), which means that the Ni and Fe components were very well dispersed over the surface of Al$_2$O$_3$, causing them to have a perfect spinel structure, as reported by Kim *et al.*[41] In addition, γ-Al$_2$O$_3$ (JCPDS 00-050-0741), Fe$_2$O$_3$ (JCPDS, 00-033-0664), and Fe$_3$O$_4$ (JCPDS, 00-019-0629) were identified in the samples.

It can be observed that increasing the calcination temperature, especially from 625 to 750 °C, leads to the Ni/Al$_3$Fe$_1$ catalyst having a more crystalline structure. A similar trend was found in the case of the ZnO–3Al catalyst, reported by Li *et al.*[27] The intensity peaks of the NiAl$_2$O$_4$ and FeAl$_2$O$_4$ increased as the calcination temperature rose in the Ni/Al$_3$Fe$_1$ catalyst. Bian *et al.*[24] reported that a high calcination temperature favored the crystal size growth.

Fig. 5(B) displays the XRD patterns of the spent samples. Our previous works[12,23] found that the phases presented in the reduced and spent catalysts were very similar except for the boehmite (AlO(OH), JCPDS 01-074-18795). For this reason, the XRD of the reduced samples is not shown in the present work. Raso *et al.*[23] found that the AlO(OH) was formed before the APH reaction and that its formation occurred during the
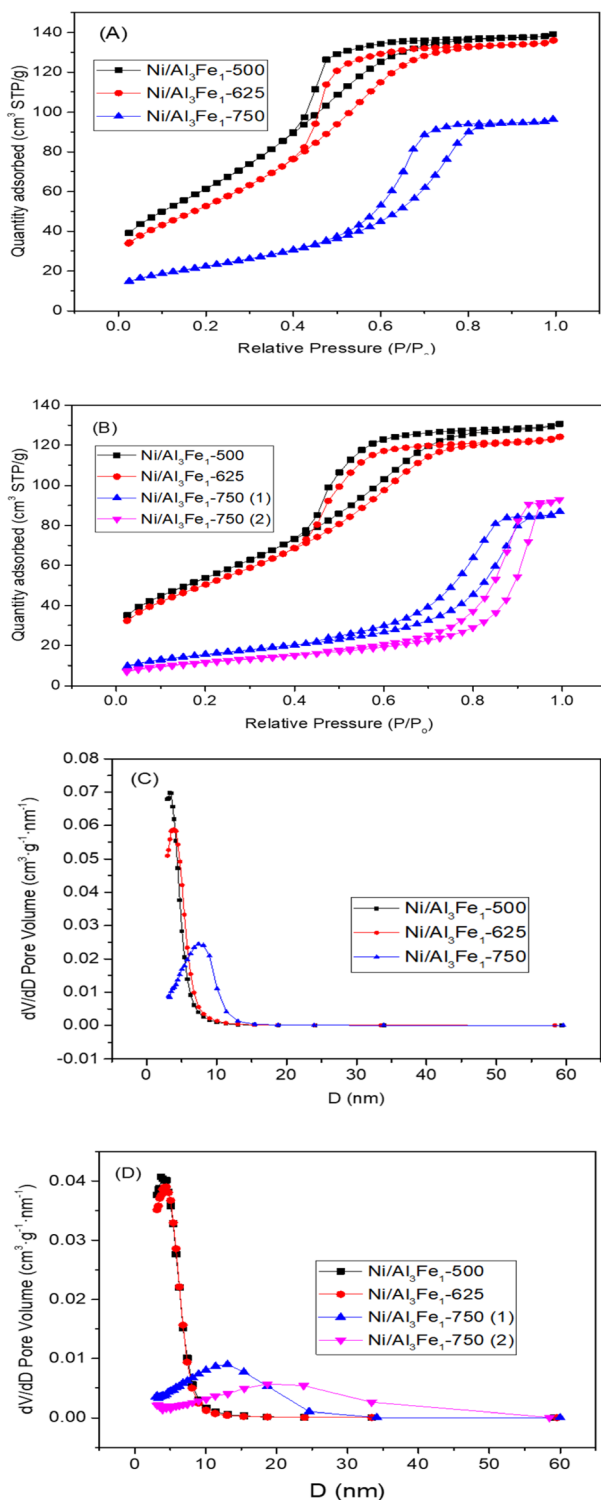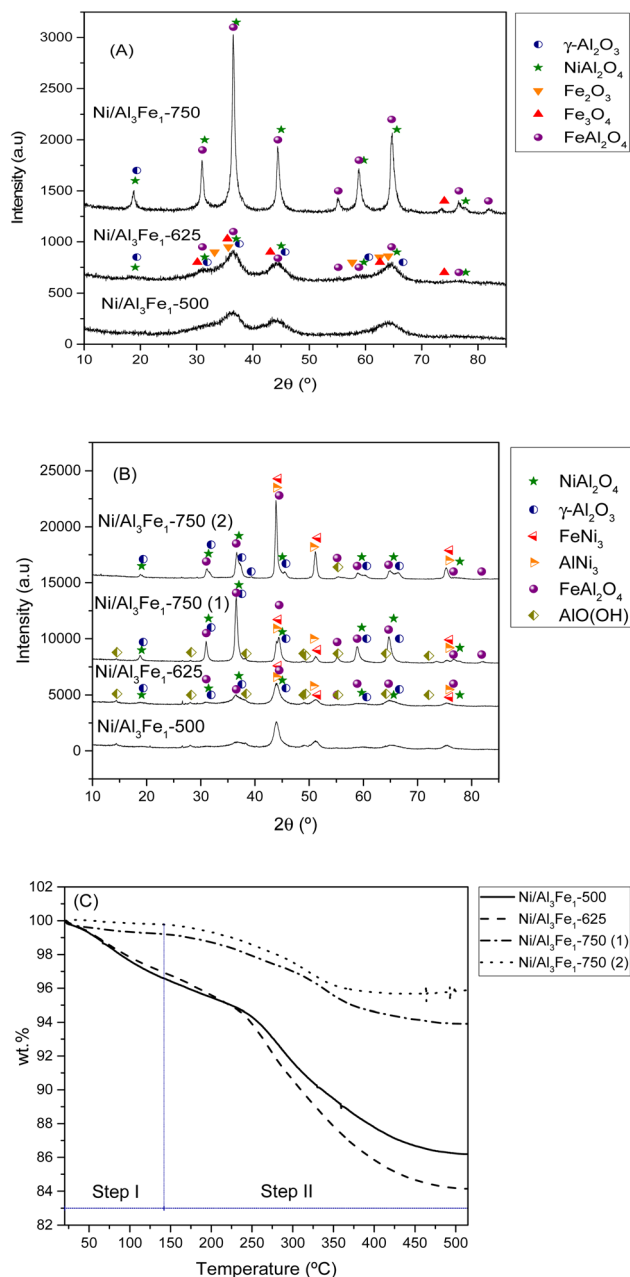
Fig. 5 XRD patterns of the calcined (A) and used (B) samples. TGA curves of the used samples (C). Step I: physisorbed water and step II: chemisorbed water and boehmite transformation.

stabilization of the system with water for the reaction. The AlO(OH) phase is formed due to the reaction between Al_2O_3 and H_2O.[13,14,23]

The principal diffraction peaks of both the $FeNi_3$ (JCPDS 03-065-3244) and $AlNi_3$ (JCPDS 00-050-1265) could be observed in all the samples due to their similar patterns.[12] Besides, the $NiAl_2O_4$ and $FeAl_2O_4$ phases were still observed due to their partial reducibility. These require a high temperature to achieve complete reduction.[41,42] However, Fe_3O_4 and Fe_2O_3 disappeared due to their total reducibility after the reduction treatment.

Increasing the reduction temperature for the Ni/Al_3Fe_1-750 catalyst from 650 °C (Ni/Al_3Fe_1-750 (1)) to 725 °C (Ni/Al_3Fe1-750

(2)) favored the reduction of the spinels ($NiAl_2O_4$ and $FeAl_2O_4$), obtaining small peaks. This means the Ni and Fe components are well combined with the Al_2O_3 support ingredient during the calcination step.[41] In addition, the intensity of the characteristic peaks of $FeNi_3$ and $AlNi_3$ was boosted with a rise in the reduction temperature. The estimated mean $FeNi_3$ crystallite sizes are shown in Table 1. Increasing the calcination temperature from 500 to 625 °C decreased the $FeNi_3$ crystallite size slightly from 8 to 7 nm, enhancing the dispersion from 12.1 to 13.9%. The dispersion was calculated using the equation $D = 97.1/d$ (nm).[43] However, a further increase in calcination temperature to 750 °C caused a decrease in the $FeNi_3$ dispersion to 8.8% due to active metal sintering during the activation process.[25] In addition, the $FeNi_3$ crystallite size increased from 11 to 20 nm when the Ni/Al_3Fe_1-750 catalyst was reduced at high temperature (725 °C), and consequently, $FeNi_3$ dispersion diminished from 8.8 to 4.9%.

Additionally, raising the calcination and reduction temperature favored decreasing the AlO(OH) phases. The approximate AlO(OH) crystallite size was 13 to 19 nm (Table 1). The presence of metal particles retards the transformation of $γ$-Al_2O_3 into AlO(OH) under hydrothermal conditions.[13] The $FeNi_3$ and AlO(OH) crystallite sizes were calculated using the Scherrer equation[44] for the characteristic diffraction peaks of $FeNi_3$ at $2θ = 44.3°$, $51.6°$, and $75.9°$ and the main peak of AlO(OH) at $2θ = 14.5°$.

According to a report by Doukkali et al.,[14] calcination treatments at high temperatures strengthen the Al–O bonds of $γ$-Al_2O_3 to minimize its interaction with the H_2O in the reaction medium, maintain the stability of the mesoporous structure and texture of the $γ$-Al_2O_3 support, and control the aggregation of Ni particles, providing higher hydrothermal stability of the catalyst in its subsequent use.

In addition, the spent samples were studied using the TGA technique in the N_2 atmosphere to quantify the boehmite formation. Fig. 5(C) shows the TGA curves of the used samples. The catalysts calcined at 500 °C and 625 °C presented higher values of total weight loss than the catalysts calcined at 750 °C. The TGA results were in good agreement with the XRD results. The weight loss is directly related to the release of adsorbed water and the transformation of boehmite (AlO(OH)) into Al_2O_3.[45] Furthermore, the boehmite formation was estimated considering the weight loss in the temperature range of 140 °C to 515 °C, which corresponded to the chemisorbed water and boehmite transformation step in the catalyst (step II). The % weight loss in step II for each sample was 10.4% for the Ni/Al_3Fe_1-500 catalyst, 12.78% for the Ni/Al_3Fe_1-625 catalyst, 5.29% for the Ni/Al_3Fe_1-750 (1) catalyst, and 3.89% for the Ni/Al_3Fe_1-750 (2) catalyst.

Looking at the catalytic results, the Ni/Al_3Fe_1-625 catalyst showed the highest catalytic activity and the smallest $FeNi_3$ crystallite size, around 7 nm, indicating a high dispersion. Increasing the calcination and reduction temperature leads to the Ni/Al_3Fe_1 catalyst having a more crystalline structure and an increased $FeNi_3$ crystallite size of around 20 nm (Ni/Al_3Fe_1-750 (2)), indicating a low dispersion.
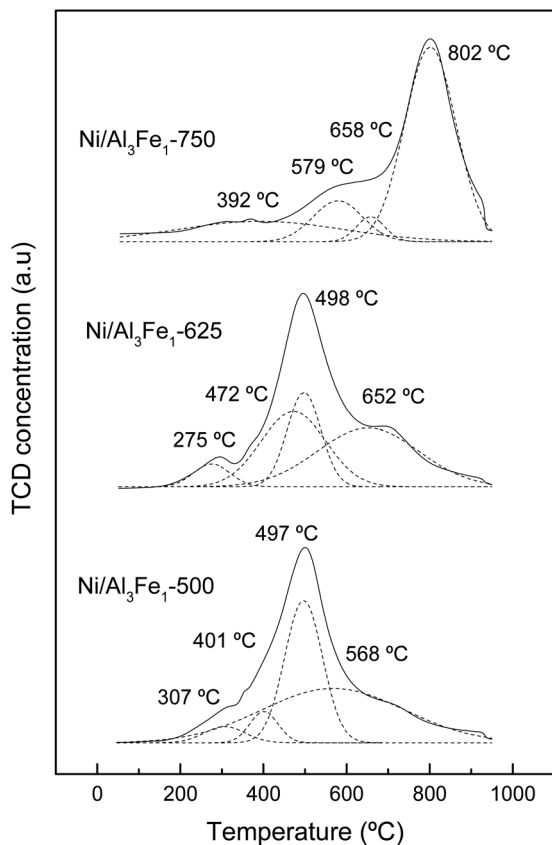
Fig. 6 H$_2$-TPR profiles of the calcined samples.

The higher amount of boehmite in the catalysts calcined at 500 and 625 °C than in the catalysts calcined at 750 °C does not appear to cause a negative effect on the catalytic activity. Furthermore, Wu *et al.*[46] used the boehmite as a support for a Cu-based catalyst in the hydrogenolysis of glycerol to 1,2-PDO.

Hydrogen temperature-programmed reduction. The H$_2$-TPR profiles of the calcined samples are depicted in Fig. 6. All the samples showed 4 peaks corresponding to the reduction of the phases present in them, obtained by the Gaussian-fitting analysis. The assignation of phases was carried out considering the XRD results.

The assignation of the peaks is in accordance with the work of Meng *et al.*[47] The peaks at low temperatures (200–440 °C) are ascribed to the reduction peak of Fe$_2$O$_3$ to Fe$_3$O$_4$ and α-NiO, the peaks at the moderate ranges (440–600 °C) are attributed to the

reduction peak of Fe$_3$O$_4$ to Fe and β-NiO, and the peaks in the range of 550–750 °C are assigned to the reduction peak of NiAl$_2$O$_4$ spinel (γ-NiO). In addition, the FeAl$_2$O$_4$ is reduced at high temperatures.[12,41]

For the Ni/Al$_3$Fe$_1$-500 and Ni/Al$_3$Fe$_1$-625 catalysts, the first peaks at 307 °C and 275 °C, respectively, might be ascribed to the reduction of α-NiO species to Ni, corresponding with the easily reducible surface free nickel oxide.[36] The second peaks at 401 °C and 472 °C for the Ni/Al$_3$Fe$_1$-500 and Ni/Al$_3$Fe$_1$-625, respectively, could be attributed to the reduction of Fe$_2$O$_3$ to Fe$_3$O$_4$. The next peaks at 497 °C and 498 °C for the Ni/Al$_3$Fe$_1$-500 and Ni/Al$_3$Fe$_1$-625, respectively, can be related to the reduction of β-NiO, which had a strong interaction with the support or referred to non-stoichiometric nickel aluminate (NiO–Al$_2$O$_3$) with weaker stability,[24,47] and Fe$_3$O$_4$ to Fe. Finally, the last peaks at 568 °C and 652 °C for the Ni/Al$_3$Fe$_1$-500 and Ni/Al$_3$Fe$_1$-625, respectively, could be assigned to the reduction of γ-NiO, which corresponded to the reduction of the NiAl$_2$O$_4$ phase or Ni phases with strong interaction with the support, and of the FeAl$_2$O$_4$ phase.

For the Ni/Al$_3$Fe$_1$-750, the first peak at 392 °C could be related to the reduction of α-NiO species. The next peak at 579 °C might be assigned to the reduction of β-NiO. The third peak at 658 °C could be attributed to the reduction of Fe$_3$O$_4$, and the last peak at 802 °C might be ascribed to the reduction of γ-NiO and FeAl$_2$O$_4$.

In addition, the ratio of the different phases was calculated and shown in Table 2. Increasing the calcination temperature decreased the proportion of α-NiO phases and β-NiO phases, whereas the ratio of γ-NiO phases was boosted. This indicated that the α-NiO and β-NiO could be converted into NiAl$_2$O$_4$, as reported by Bian *et al.*[24] They stated that increasing the calcination temperature favored the NiAl$_2$O$_4$ formation, which was beneficial for the dry reforming of methane in terms of activity and stability.

Moreover, the reduction temperature peaks moved towards higher values with the increase in the calcination temperature. For example, the reduction temperature peaks of the γ-NiO/FeAl$_2$O$_4$ species were boosted from 568 °C to 802 °C with the rise of the calcination temperature from 500 °C to 750 °C.

Temperature-programmed desorption of ammonia. Temperature-programmed desorption of ammonia (NH$_3$-TPD) was carried out to study the acidity of the reduced catalysts. A Gaussian-fitting analysis was conducted to clarify the kinds of desorption regions in the catalysts. The results of NH$_3$-TPD are gathered in Table 3.

Table 2 H$_2$-TPR results of the calcined samples

| Sample | Reduction temperature (°C)/relative content[b] (%) | | | | | Total H$_2$ consumption (mmol H$_2$/g$_{cat}$) |
	α-NiO	Fe$_2$O$_3$	β-NiO	Fe$_3$O$_4$	γ-NiO/FeAl$_2$O$_4$	
Ni/Al$_3$Fe$_1$-500	307/5.5	401/7.3	497/41.4[a]		568/45.8	9.25
Ni/Al$_3$Fe$_1$-625	275/4.1	472/25.0	498/27.3[a]		652/43.6	9.21
Ni/Al$_3$Fe$_1$-750	392/3.8		579/16.8	658/5.4	802/74.0	9.45

[a] Value corresponding to a total reduction of β-NiO and Fe$_3$O$_4$. [b] Calculated from Gaussian deconvolution of H$_2$-TPR.
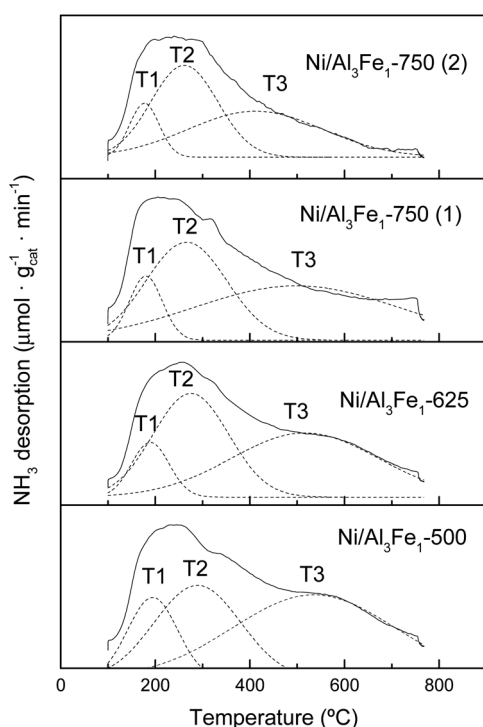
Table 3 NH$_3$-TPD results of the reduced samples and crystallite size of used samples calculated from STEM results

| Sample	Temperature (°C)/relative amount^a (%)			Total NH$_3$ desorption (μmol NH$_3$/g$_{cat}$)	STEM^b (nm)
	T1/F1	T2/F2	T3/F3		
Ni/Al$_3$Fe$_1$-500	194/21.4	289/36.9	536/41.8	777.34	11
Ni/Al$_3$Fe$_1$-625	189/10.3	275/39.5	516/50.2	881.54	10
Ni/Al$_3$Fe$_1$-750 (1)	180/13.9	266/42.0	498/44.1	433.24	20
Ni/Al$_3$Fe$_1$-750 (2)	177/10.6	261/43.7	411/45.7	337.43	41

^{a} Calculated from Gaussian deconvolution of NH$_3$-TPD profiles. ^{b} Mean particle size calculated from STEM results.

The NH$_3$-TPD profiles of the reduced catalyst are shown in Fig. 7. Previous to the NH$_3$-TPD analysis, the samples were reduced at the same temperature as that used to activate them before the APH reaction: 500 °C for the Ni/Al$_3$Fe$_1$-500 and Ni/Al$_3$Fe$_1$-625, 650 °C for the Ni/Al$_3$Fe$_1$-750 (1) and 725 °C for the Ni/Al$_3$Fe$_1$-750 (2). All catalysts presented three regions characteristic of the strength of the acid sites with maxima at the ranges 177–194 °C, 261–289 °C, and 411–536 °C, corresponding to weak (T1), low-moderate (T2), and strong (T3), respectively.

The proportion of the low-moderate (F2) and strong (F3) acid sites rose when the calcination temperature increased from 500 to 625 °C. Then, raising the calcination temperature to 750 °C favored increasing the proportion of the low-moderate acid sites and decreasing the strong acid sites. In addition, boosting the activation temperature of the Ni/Al$_3$Fe$_1$-750 from 650 (Ni/Al$_3$Fe$_1$-750 (1)) to 725 °C (Ni/Al$_3$Fe$_1$-750 (2)) slightly increased the proportion of the low-moderate and strong acid sites, but diminished the temperature of these acid sites, especially the strong acid sites.

The total amount of acid sites increased slightly from 777.34 to 881.54 μmol NH$_3$/g$_{cat}$ when the calcination temperature was raised from 500 to 625 °C, respectively. However, raising it to 750 °C decreased half of the total amount of acid sites. In addition, increasing the reduction temperature from 650 to 725 °C reduced the amount of acid sites from 433.24 to 337.43 μmol NH$_3$/g$_{cat}$, respectively.
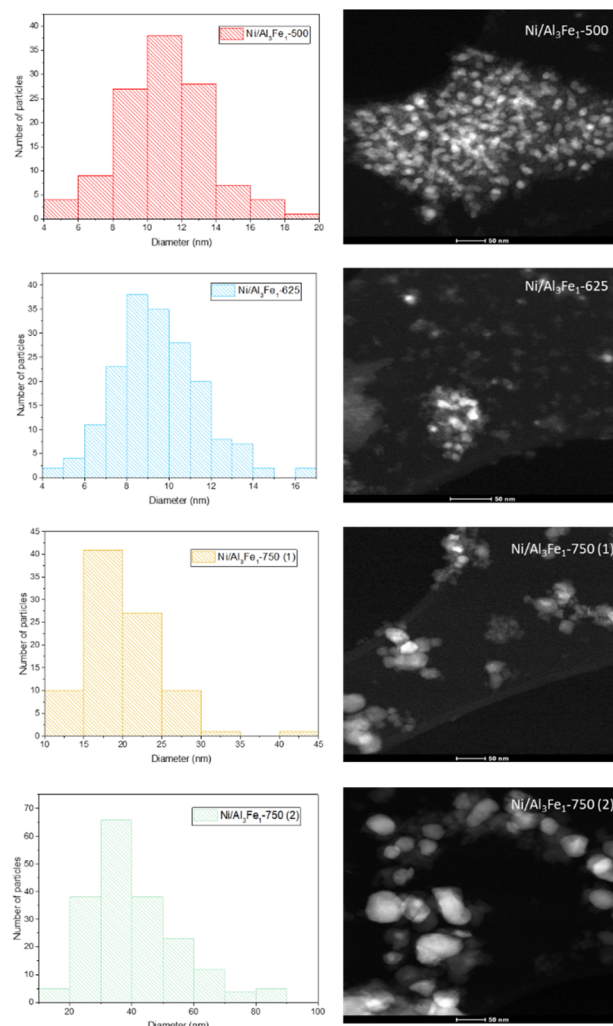
Fig. 8 The nickel-rich particle size distribution and STEM images of the used catalysts.

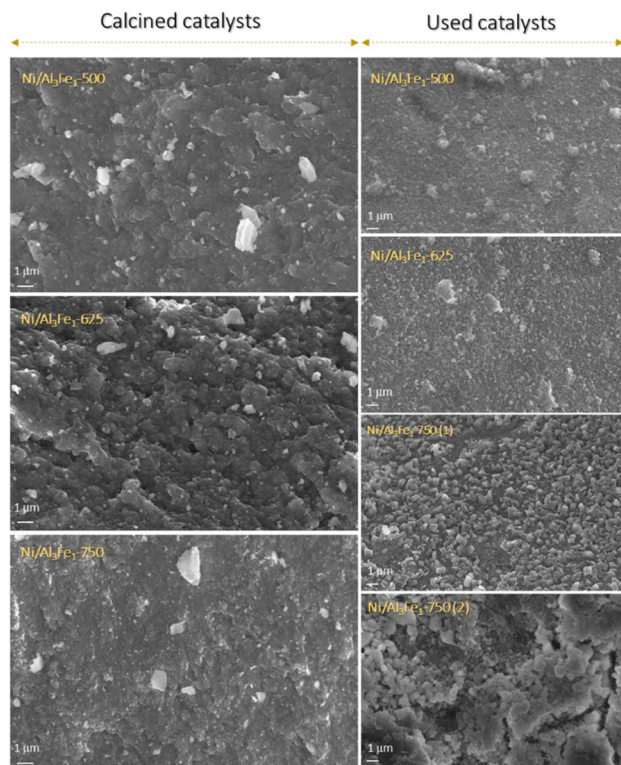**Fig. 7** NH$_3$-TPD profiles of the reduced samples.

Fig. 9 FESEM images of the calcined and used catalysts from left to right.

Scanning transmission electron microscopy. Scanning transmission electron microscopy (STEM) was applied to determine the metal crystallite sizes of the samples. Fig. 8 shows the nickel-rich particle size distribution of the catalysts, calculated by image processing software. More than 90 particles were measured per sample. The estimated nickel-rich particle size was 10 to 41 nm (Table 3).

The same trend of the particle sizes obtained by the XRD technique was observed with the STEM technique. Increasing the calcination temperature from 500 to 625 °C decreased the nickel-rich crystallite size slightly from 11 to 10 nm, improving the dispersion. The Ni/Al$_3$Fe$_1$-500 and Ni/Al$_3$Fe$_1$-625 catalysts showed around 34% and 63% of nickel-rich particle sizes below 10 nm, respectively. This corroborates the XRD results and the higher dispersion of the nickel-rich phase on the Ni/Al$_3$Fe$_1$-625 catalyst compared to the Ni/Al$_3$Fe$_1$-500 catalyst. A further

increase in calcination temperature to 750 °C caused a diminution in the nickel-rich phase dispersion. In addition, the nickel-rich crystallite size increased from 20 to 41 nm when the Ni/Al$_3$Fe$_1$-750 was reduced at high temperatures, and its dispersion subsequently decreased.

Field emission scanning electron microscopy. Field emission scanning electron microscopy (FESEM) images of the samples are displayed in Fig. 9. The morphology of the catalysts changed after their use due to the presence of the boehmite, as identified by the XRD technique.

The variations in the morphology depended on the operating conditions, such as hydrothermal temperature, treatment time, and reactant concentrations. The morphologies included cubes, elongated shapes, thick plates, and platelet-like or flower-like particles.[48,49]

Additionally, elemental analysis of the spent catalysts was performed in order to determine coke formation. Increasing the calcination temperature favored the coke formation expressed using the ratio mg C/(g$_{catalyst}$·g$_{glycerol\ reacted}$) in the Ni/Al$_3$Fe$_1$ catalyst (1.99 to 4.29 mg C/(g$_{catalyst}$·g$_{glycerol\ reacted}$)). Meanwhile, boosting the reduction temperature from 650 to 725 °C slightly decreased the coke formation, 4.29 to 3.92 mg C/(g$_{catalyst}$·g$_{glycerol\ reacted}$) (Table 4). The H content in the used catalysts follows a similar trend to the TGA results (% total weight loss) and could be related to boehmite formation.

Discussion

This study aimed to optimize the calcination temperature of the Ni/Al$_3$Fe$_1$ catalyst in the APH of glycerol without external hydrogen addition. In this context, Ni/Al$_3$Fe$_1$ catalysts calcined at different temperatures (500, 625, and 750 °C) were prepared by the co-precipitation method and tested in the APH of glycerol under the same operating conditions.

The results showed that the Ni/Al$_3$Fe$_1$ catalyst calcined at 625 °C presented the best catalytic activity, obtaining a glycerol conversion of around 53%. The proportion of the carbon selectivity to liquid (80%) and gas (20%) products is the same for all catalysts. This could mean the calcination or reduction temperatures did not affect this distribution. Then, the total carbon selectivity to liquid and gas products is determined by the operating conditions, and the catalyst is also influenced. Thus, Garcia *et al.*[30] obtained about 25% and 75% of total carbon selectivity to gas and liquid products, respectively, during the APR of glycerol over Ni/Al coprecipitated catalyst under the same operating conditions (34 bar, 10 wt% glycerol, and 227 °C). The higher carbon selectivity to liquids with the Ni/Al$_3$Fe$_1$ catalyst than with the Ni/Al catalyst could indicate the positive effect of Fe.

The yield to 1,2-PDO, the main liquid product, was 209 mg g^{-1} glycerol and 192 mg g^{-1} glycerol for the catalysts calcined at 625 and 500 °C, respectively. The H$_2$ yield, expressed as mg H$_2$/mol C fed, was 47 and 34 for these catalysts, respectively. These results indicate a slight improvement using the catalyst calcined at 625 °C. On the other hand, the catalyst calcined at 750 °C and reduced at two different temperatures (650 and 725 °C) showed low catalytic activity with a 1,2-PDO yield of

Table 4 Elemental analysis results of the used catalysts

	C (wt%)	H (wt%)	Ratio (mg C/(g$_{catalyst}$·g$_{glycerol}$ reacted))
Ni/Al$_3$Fe$_1$-500	1.77	0.88	1.99
Ni/Al$_3$Fe$_1$-625	2.72	0.90	3.01
Ni/Al$_3$Fe$_1$-750 (1)	1.74	0.41	4.29
Ni/Al$_3$Fe$_1$-750 (2)	1.52	0.31	3.92

around 35 mg g^{-1} glycerol for both catalysts and an H$_2$ yield of 13 and 19 mg H$_2$/mol C fed for the catalysts reduced at 650 and 725 °C, respectively.

The conversion of glycerol is due to reforming reactions that produce gases and liquid phase reactions, mainly by path I (eqn (6)) and path II (eqn (7)).[30–32] The acid sites of the catalysts participate in path I by dehydrating glycerol to acetol. In contrast, metal sites of the catalysts are involved in reforming reactions that generate hydrogen and path II by the dehydrogenation/decarbonylation of glycerol.[13]

The catalysts calcined at low temperatures, 500 °C and 625 °C, presented a high value of acidity and a small size of Ni-rich phase, both favoring the glycerol conversion. The simultaneous reforming reaction of glycerol that produces hydrogen and its participation in the hydrogenation of acetol explained the high 1,2-PDO yield obtained with these catalysts.

In addition, the H$_2$/CO$_2$ ratio in the product gas with the catalysts calcined at 500 and 625 °C was 0.25 and 0.30, respectively, which was significantly lower than 7/3 of the stoichiometric ratio of glycerol reforming, corroborating the participation of hydrogen in liquid phase reactions.[36]

With the purpose of increasing the knowledge of the influence of the calcination temperature on reaction routes in a liquid phase, Table 5 shows the total carbon selectivity to the main products of path I, acetol and 1,2-PDO, and the total carbon selectivity to the main products of path II, ethylene glycol and ethanol. It is observed that the main reaction route was path I for all the catalysts tested. Moreover, the total carbon selectivity to path I decreased with the increase in the calcination temperature and the reduction temperature using the catalyst calcined at 750 °C. On the other hand, the total carbon selectivity to the products of path II increased with the calcination and reduction temperatures. The tendency observed with the reduction temperature was found previously by Morales-Marin et al.[36] in their study of the effect of the reduction temperature on the APR of glycerol over NiAl$_2$O$_4$-derived catalysts. They concluded that the reduction at 700 °C or above enhanced the dehydrogenation mechanism, while the catalysts reduced at below 600 °C favored dehydration/hydrogenation products.

Table 5 also shows the ratio of total carbon selectivity to 1,2-PDO/acetol for the catalysts tested. This ratio is directly related to the hydrogenation activity and was significantly higher for the catalysts calcined at 500 °C and 625 °C. The small size of the Ni-rich phase of these catalysts produced more hydrogen and favored the hydrogenation of acetol to 1,2-PDO.

Freitas et al.[13] found that bimetallic CuNi/Al$_2$O$_3$ and CuNi/ZSM-5 catalysts displayed the highest glycerol conversion, 80% and 85%, respectively, with 25% of 1,2-PDO yield at 250 °C and 40 bar, without external hydrogen. They attributed this result to Cu–Ni alloy interaction, high acidity, and good metal dispersion on the catalyst.

Barzegari et al.[25] reported that the active surface area and Ni dispersion were gradually diminished by boosting the calcination temperature from 600 to 700 °C. In addition, the catalyst calcined at 600 °C showed the highest catalytic activity. This tendency is in accordance with the results obtained with the Ni/Al$_3$Fe$_1$ catalysts.

Overall, the high catalytic activity for the APH of glycerol without external hydrogen addition was favored with high acidity and good metal dispersion on the catalyst. In this case, the Ni/Al$_3$Fe$_1$-625 catalyst was selected as the best due to its high acidity, high metal dispersion, and lower metal leaching than the Ni/Al$_3$Fe$_1$-500 catalyst. Thus, the Ni/Al$_3$Fe$_1$-625 catalyst demonstrated the best catalytic activity, obtaining the most significant results of H$_2$ and 1,2-PDO yields. Path I was favored at a low calcination temperature (below 625 °C) because the Ni/Al$_3$Fe$_1$-625 catalyst showed the highest acidity and metal dispersion. Besides, increasing the calcination temperature to 750 °C enhanced the selectivity of dehydrogenation products (EG + ethanol) and decreased the H$_2$ yield. At the same calcination temperature (750 °C), boosting the reduction temperature from 650 to 725 °C favored both the selectivity of dehydrogenation products (EG + ethanol) and the H$_2$ yield. This could mean path II was enhanced at high calcination and reduction temperatures (above 725 °C).

Conclusions

An increase in the calcination temperature from 500 to 750 °C produced a significant change in the physicochemical properties of the Ni/Al$_3$Fe$_1$ catalyst and its catalytic activity during the APH of glycerol.

The calcined catalyst's surface area was decreased from 233 to 82 m^2 g^{-1} with an increase in the calcination temperature; meanwhile, the pore diameter was increased from 3.3 to 7.4 nm. After its use, acceptable stability in the surface area and pore diameter were observed for the Ni/Al$_3$Fe$_1$ catalysts calcined at 500 °C and 625 °C, while a significant decrease in surface area and increase in pore diameter were determined for the catalyst calcined at 750 °C.

The Ni/Al$_3$Fe$_1$-625 catalyst was selected as the best due to its high acidity, metal dispersion, and catalytic activity, the highest carbon selectivity product being 1,2-PDO. In addition, it experienced less metal leaching than the Ni/Al$_3$Fe$_1$-500 catalyst.

Author contributions

R. Raso: investigation, methodology, formal analysis, validation, visualization, writing – original draft. A. Lete: investigation, validation. L. García: conceptualization, supervision, writing – review & editing, funding acquisition. J. Ruiz: methodology, formal analysis, writing – review & editing. M. Oliva:

Table 5 Total carbon selectivity to path I and path II, ratio $S_{1,2\text{-PDO}}/S_{\text{acetol}}$

	Path I (acetol + 1,2-PDO)	Path II (ethylene glycol + ethanol)	$S_{1,2\text{-PDO}}/S_{\text{acetol}}$
Ni/Al$_3$Fe$_1$-500	61.3	17.5	6.8
Ni/Al$_3$Fe$_1$-625	60.2	17.8	7.2
Ni/Al$_3$Fe$_1$-750 (1)	57.7	22.5	1.8
Ni/Al$_3$Fe$_1$-750 (2)	51.7	27.7	2.4

conceptualization, writing – review & editing. J. Arauzo: supervision, writing – review & editing, funding acquisition.

Conflicts of interest

There are no conflicts of interest to declare.

Acknowledgements

References

1 Y. Guo, M. Azmat, X. Liu, Y. Wang and G. Lu, *Appl. Energy*, 2012, **92**, 218–223.

2 F. Akram, I. ul Haq, S. Raja, A. Mir, S. Qureshi, A. Aqeel and F. Shah, *J. Cleaner Prod.*, 2022, **370**, 133479.

3 H. Pan, Q. Xia, Y. Wang, Z. Shen, H. Huang, Z. Ge, X. Li, J. He, X. Wang, L. Li and Y. Wang, *Fuel Process. Technol.*, 2022, **237**, 107421.

4 T. Mahlia, Z. Syazmi, M. Mofijur, A. Abas, M. Bilad, H. Ong and A. Silitonga, *Renewable Sustainable Energy Rev.*, 2020, **118**, 109526.

5 S. Chozhavendhan, M. V. P. Singh, B. Fransila, R. P. Kumar and G. K. Devi, *Curr. Res. Green Sustainable Chem.*, 2020, **1–2**, 1–6.

6 M. K. Awasthi, S. Sarsaiya, A. Patel, A. Juneja, R. P. Singh, B. Yan, S. K. Awasthi, A. Jain, T. Liu, Y. Duan, A. Pandey, Z. Zhang and M. J. Taherzadeh, *Renewable Sustainable Energy Rev.*, 2020, **127**, 109876.

7 R. Cortright, R. Davda and J. Dumesic, *Nature*, 2002, **418**, 964–967.

8 N. Pandhare, S. Pudi, P. Biswas and S. Sinha, *J. Taiwan Inst. Chem. Eng.*, 2016, **61**, 90–96.

9 V. Yfanti, E. Vasiliadou, S. Sklari and A. Lemonidou, *J. Chem. Technol. Biotechnol.*, 2017, **92**, 2236–2245.

10 Y. Nakagawa and K. Tomishige, *Catal. Sci. Technol.*, 2011, **1**, 179–190.

11 A. Gonzalez-Garay, M. Gonzalez-Miquel and G. Guillen-Gosalbez, *ACS Sustainable Chem. Eng.*, 2017, **5**, 5723–5732.

12 R. Raso, L. Garcia, J. Ruiz, M. Oliva and J. Arauzo, *Appl. Catal., B*, 2021, **283**, 119598.

13 I. Freitas, R. Manfro and M. Souza, *Appl. Catal., B*, 2018, **220**, 31–41.

14 M. El Doukkali, A. Iriondo, N. Miletic, J. Cambra and P. Arias, *Int. J. Hydrogen Energy*, 2017, **42**, 23617–23630.

15 R. Chimentao, B. Miranda, D. Ruiz, F. Gispert-Guirado, F. Medina, J. Llorca and J. Santos, *J. Energy Chem.*, 2020, **42**, 185–194.

16 E. D'Hondt, S. de Vyver, B. Sels and P. Jacobs, *Chem. Commun.*, 2008, 6011–6012.

17 D. Roy, B. Subramaniam and R. Chaudhari, *Catal. Today*, 2010, **156**, 31–37.

18 A. Seretis and P. Tsiakaras, *Fuel Process. Technol.*, 2016, **142**, 135–146.

19 A. Soares, G. Perez and F. Passos, *Appl. Catal., B*, 2016, **185**, 77–87.

20 M. Dasari, P. Kiatsimkul, W. Sutterlin and G. Suppes, *Appl. Catal., A*, 2005, **281**, 225–231.

21 F. Cai, D. Pan, J. Ibrahim, J. Zhang and G. Xiao, *Appl. Catal., A*, 2018, **564**, 172–182.

22 V. G. S. Mendonça, I. C. Freitas, R. L. Manfro and M. M. V. M. Souza, *Appl. Catal., A*, 2022, **645**, 118838.

23 R. Raso, L. Garcia, J. Ruiz, M. Oliva and J. Arauzo, *Catalysts*, 2020, **10**, 1482.

24 Z. Bian, W. Zhong, Y. Yu, Z. Wang, B. Jiang and S. Kawi, *Int. J. Hydrogen Energy*, 2021, **46**, 31041–31053.

25 F. Barzegari, M. Kazemeini, M. Rezaei, F. Farhadi and A. Keshavarz, *Fuel*, 2022, **322**, 124211.

26 H. Ozdemir, M. Oksuzomer and M. Gurkaynak, *Fuel*, 2014, **116**, 63–70.

27 X. Li, Q. Wu, B. Zhang, C. Zhang, W. Lin, H. Cheng and F. Zhao, *Catal. Today*, 2018, **302**, 210–216.

28 N. Hamzah, W. Z. a. Y. ABD Samad and M. Ambar, *Mater. Sci. Forum*, 2017, **888**, 518–523.

29 Z. Xiao, S. Jin, X. Wang, W. Li, J. Wang and C. Liang, *J. Mater. Chem.*, 2012, **22**, 16598.

30 L. Garcia, A. Valiente, M. Oliva, J. Ruiz and J. Arauzo, *Int. J. Hydrogen Energy*, 2018, **43**, 20392–20407.

31 K. Wu, B. Dou, H. Zhang, D. Liu, H. Chen and Y. Xu, *Fuel*, 2022, **308**, 122014.

32 K. Wu, B. Dou, H. Zhang, D. Liu, H. Chen and Y. Xu, *J. Energy Inst.*, 2021, **99**, 198–208.

33 J. Remon, J. Gimenez, A. Valiente, L. Garcia and J. Arauzo, *Energy Convers. Manage.*, 2016, **110**, 90–112.

34 M. L. Meena, H. Malviya, N. N. Pandhare and P. Biswas, *Curr. Res. Green Sustainable Chem.*, 2022, **5**, 100289.

35 A. Arandia, I. Coronado, A. Remiro, A. Gayubo and M. Reinikainen, *Int. J. Hydrogen Energy*, 2019, **44**, 13157–13168.

36 A. Morales-Marin, J. Ayastuy, U. Iriarte-Velasco, M. Gutierrez-Ortiz and C. T. Environm, *Appl. Catal., B*, 2019, **244**, 931–945.

37 A. Reynoso, J. Ayastuy, U. Iriarte-Velasco, M. Gutierrez-Ortiz and C. T. Environm, *Appl. Catal., B*, 2018, **239**, 86–101.

38 M. Thommes, K. Kaneko, A. Neimark, J. Olivier, F. Rodriguez-Reinoso, J. Rouquerol and K. Sing, *Pure Appl. Chem.*, 2015, **87**, 1051–1069.

39 L. E. Alzamora, J. R. H. Ross, E. C. Kruissink and L. L. Van Reijen, *J. Chem. Soc., Faraday Trans. 1*, 1981, **77**, 665–681.

40 J. Chen, L. Yu, J. Sun, Y. Li and W. Xue, *J. Eur. Ceram. Soc.*, 2011, **31**, 259–263.

41 K. Kim, B. Kwak, N. Park, T. Lee, S. Lee and M. Kang, *Ind. Eng. Chem.*, 2017, **46**, 324–336.

42 D. Shi, R. Wojcieszak, S. Paul and E. Marceau, *Catalysts*, 2019, **9**, 451.

43 L. Wang, D. Li, M. Koike, S. Koso, Y. Nakagawa, Y. Xu and K. Tomishige, *Appl. Catal., A*, 2011, **392**, 248–255.

44 V. Uvarov and I. Popov, *Mater. Charact.*, 2013, **85**, 111–123.

45 M. Mirzaee, M. Amini, M. Sadeghi, F. Mousavi and M. Sharbatdaran, *Ceram.-Silik.*, 2005, **49**, 40–47.

46 Z. Wu, Y. Mao, M. Song, X. Yin and M. Zhang, *Catal. Commun.*, 2013, **32**, 52–57.

47 F. Meng, P. Zhong, Z. Li, X. Cui and H. Zheng, *J. Chem.*, 2014, 534842.

48 R. Denigres, G. Rocha, C. Montes and A. Vieira-Coelho, *Mater. Res.*, 2016, **19**, 659–668.

49 Z. Wang, Y. Tian, H. Fan, J. Gong, S. Yang, J. Ma and J. Xu, *New J. Chem.*, 2014, **38**, 1321–1327.